JOURNAL OF GEOPHYSICAL RESEARCH, VOL. 113, D17117, doi:10.1029/2008JD009786, 2008

Wintertime temperature maximum at the subtropical stratopause in a T213L256 GCM

Y. Tomikawa,[1] K. Sato,[2] S. Watanabe,[3] Y. Kawatani,[3] K. Miyazaki,[3] and M. Takahashi[3,4]

Received 4 January 2008; revised 30 April 2008; accepted 9 June 2008; published 10 September 2008.

[1] A wintertime temperature maximum can be observed at the subtropical stratopause but does not appear in the radiative equilibrium temperature distribution. This structure was well simulated using a high-resolution general circulation model and examined in detail. The stratopause temperature is latitudinally maximized in the winter subtropics because of a strong downwelling of the meridional circulation from summer tropics to winter subtropics passing above the stratopause. Its strong meridional flow consists of two parts: a strong poleward flow in the winter subtropics with nearly vertically aligned contours of absolute angular momentum (M) and a strong cross-equatorial flow toward winter hemisphere above the tropical stratopause with nearly horizontally aligned M contours. The strong poleward flow in the winter subtropics is driven by a large Eliassen-Palm (E-P) flux convergence in a small absolute vorticity region. The large E-P flux convergence is due to extratropical planetary waves and asymmetric inertial instability. On the other hand, the strong cross-equatorial flow is induced along the M contour to satisfy mass continuity with the strong poleward flow in the winter subtropics and exists in the easterly phase of S-SAO with a small latitudinal gradient of M. The easterly of S-SAO during its mature phase acts as a corridor for cross-equatorial meridional circulation, while cross-equatorial meridional circulation contributes to driving the easterly of S-SAO in its development phase.

Citation: Tomikawa, Y., K. Sato, S. Watanabe, Y. Kawatani, K. Miyazaki, and M. Takahashi (2008), Wintertime temperature maximum at the subtropical stratopause in a T213L256 GCM, *J. Geophys. Res.*, *113*, D17117, doi:10.1029/2008JD009786.

1. Introduction

[2] Gravity waves play a primary role in determining large-scale temperature and wind distributions in the middle atmosphere, along with planetary waves. Their role and behavior have been investigated on the basis of both observations and model experiments. Radiosonde observations conducted globally in the last several decades have helped us to understand basic characteristics, seasonal variations, and spatial distributions of gravity waves [*Kitamura and Hirota*, 1989; *Allen and Vincent*, 1995; *Sato and Dunkerton*, 1997; *Sato et al.*, 2003; *Yoshiki and Sato*, 2000; *Yoshiki et al.*, 2004]. Mesosphere-Stratosphere-Troposphere (MST) radars, which measure three-dimensional wind speeds with high vertical (O(100) m) and temporal (O(1) min) resolutions, make it possible to directly estimate the vertical momentum flux associated with gravity waves in the lower stratosphere and mesosphere [*Tsuda et al.*, 1990; *Sato*, 1994]. Recent satellite measurements of temperature provide global coverage of gravity wave activity in the stratosphere and mesosphere [*Fetzer and Gille*, 1994; *Wu and Waters*, 1996; *Eckermann and Preusse*, 1999; *Tsuda et al.*, 2000; *Ern et al.*, 2004], though they cover a limited spectral range of gravity waves [*Alexander*, 1998]. Lidar measurements are the only ground-based method by which potential energy distribution of gravity waves in the upper stratosphere and mesosphere can be obtained with a relatively high vertical resolution of O(1000) m [*Wilson et al.*, 1991; *Duck et al.*, 2001; *Blum et al.*, 2004]. However, it is still impossible to determine the global distribution of the whole spectrum of gravity waves even with state-of-the-art observational techniques.

[3] The effects of gravity waves (i.e., momentum transfer and deposit) are usually parameterized in general circulation models (GCMs) because their horizontal and vertical resolutions are not sufficient to explicitly resolve the gravity waves. Insufficient representation of gravity wave source, propagation, and dissipation results in some unrealistic features of temperature and wind distributions in the GCMs, such as a cold bias in the polar stratosphere [cf., *Pawson et al.*, 2000]. On the other hand, some attempts to examine the effects and behavior of explicitly resolved gravity waves in the GCMs have been performed since the late 1990s. *Takahashi* [1996, 1999] successfully reproduced a quasi-biennial oscillation (QBO)-like oscillation in the tropical

[1]National Institute of Polar Research, Tokyo, Japan.
[2]Department of Earth and Planetary Science, Graduate School of Science, University of Tokyo, Tokyo, Japan.
[3]Frontier Research System for Global Change/JAMSTEC, Kanagawa, Japan.
[4]Center for Climate System Research, University of Tokyo, Chiba, Japan.

0148-0227/08/2008JD009786$09.00

stratosphere using a GCM without parameterizing nonorographic gravity waves. *Sato et al.* [1999] showed a global view of horizontal and vertical propagation of spontaneously generated gravity waves and their associated spectral peaks at the inertial period of each latitude in a high-resolution GCM with an aquaplanet boundary condition. High-resolution GCMs (e.g., T106L60, which is approximately equivalent to 1.125° longitude-latitude grid and 550-m vertical resolution) with a realistic topography have also been adopted to examine global and local features of spontaneously generated gravity waves [e.g., *Kawatani et al.*, 2003, 2004, 2005; *Watanabe et al.*, 2006].

[4] This historical background based on observational and GCM studies prompted us to perform a model experiment using a GCM with a resolution high enough (and higher than in previous experiments) to explicitly resolve the gravity waves. This group study was named "KANTO Project". The main objectives of the KANTO Project were to understand the effects of small-scale phenomena such as gravity waves on large-scale circulation in the middle atmosphere using a high-resolution GCM [*Watanabe et al.*, 2008].

[5] The tropical middle atmosphere supports a semiannual oscillation of zonal-mean zonal wind at the stratopause (S-SAO), as well as the QBO. The S-SAO was discovered by *Reed* [1962, 1966] through radiosonde and rocketsonde observations. A westerly phase of the S-SAO has been attributed to westerly momentum deposition by Kelvin [*Hirota*, 1978, 1980; *Hitchman and Leovy*, 1988] and gravity waves [*Müller et al.*, 1997]. An easterly phase of the S-SAO is induced partly by easterly momentum deposition due to planetary waves propagating into the tropics [*Hirota*, 1980] and gravity waves [*Ray et al.*, 1998]. In addition, easterly momentum advection due to the meridional circulation contributes to the easterly acceleration of the S-SAO [*Holton and Wehrbein*, 1980].

[6] A time-mean (i.e., monthly or seasonal) meridional circulation across nearly vertically aligned contours of absolute angular momentum (M) in the extratropics is driven by a wave-induced torque to maintain the thermal wind balance [*Eliassen*, 1951; *Garcia*, 1987; *Haynes et al.*, 1991]. Such a wave-driven meridional circulation exists also in the tropics [*Plumb and Eluszkiewicz*, 1999]. However, there is another type of meridional circulation in the tropics where the latitudinal gradients of M are relatively small due to the small magnitude of the Coriolis parameter. The tropical stratopause region supports a middle atmosphere Hadley circulation from the summer to winter hemisphere during solstice seasons, to counteract a significant latitudinal gradient of radiative equilibrium temperature through its adiabatic heating/cooling [*Dunkerton*, 1989; *Semeniuk and Shepherd*, 2001a, 2001b]. The momentum advection due to the middle atmosphere Hadley circulation would contribute to driving an easterly phase of the S-SAO because of strong nonlinearity around the tropical stratopause [*Dunkerton*, 1991]. The easterly phase of S-SAO is associated with nearly horizontally aligned contours of M around the tropical stratopause. Even if there is no wave-induced torque in the tropics, the meridional circulation can go through the region with nearly horizontally aligned contours of M. Direction and strength of the meridional flow across such a region are controlled by the direction and strength of the meridional flow in the extratropics on the same M contours, which is called "sideways control" [*Hitchman and Leovy*, 1986; *Dunkerton*, 1989; *Tung and Kinnersley*, 2001]. These three types of meridional circulation (i.e., wave-driven and middle atmosphere Hadley circulation, and sideways control) coexist in the tropical middle atmosphere. However, when and to what extent each mechanism contributes to the total meridional circulation in the tropical middle atmosphere remains undetermined. This study demonstrates that the "sideways control" mechanism dominates around solstice seasons above the tropical stratopause.

[7] The focus of the present work is on zonal-mean temperature and wind distributions around the stratopause in the tropics and subtropics. A close relationship between the zonal-mean temperature and wind structures, residual-mean meridional circulation, and the subtropical wave-induced torque is examined in terms of the transformed Eulerian-mean formalism and the absolute angular momentum distribution. The remainder of this paper is organized as follows. An experimental setup and general features of the GCM are described in section 2. A good correspondence between the temperature maximum and strong downwelling of the meridional circulation is shown in section 3. A mechanism driving the strong meridional circulation above the stratopause in the tropics and winter subtropics is discussed in terms of the absolute angular momentum distribution and subtropical wave-induced torque in section 4. Waves imposing the torque around the stratopause in the winter subtropics are examined in section 5. Concluding remarks are given in section 6.

2. Model Description

[8] The CCSR/NIES/FRCGC AGCM version 5.7b used in this study is based on an atmospheric component of a coupled ocean-atmosphere GCM called MIROC (Model for Interdisciplinary Research on Climate) version 3.2, which has been developed at the Center for Climate System Research, the University of Tokyo (CCSR), National Institute for Environmental Studies (NIES) and Frontier Research Center for Global Change (FRCGC) [*K-1 model developers*, 2004; *Nozawa et al.*, 2007]. Many model setups in the CCSR/NIES/FRCGC AGCM have been modified and extended for this study [*Watanabe et al.*, 2008]. The GCM is a T213 (i.e., approximately equivalent to 0.5625° longitude-latitude grid) global atmospheric spectral model with 256 vertical levels from the ground to an altitude of 85 km with a vertical spacing of about 300 m in the stratosphere and mesosphere. A ratio of the horizontal to vertical resolution (i.e., $\sim$150) is approximately equivalent to Prandtl's ratio ($\equiv N/f$) for quasi-geostrophic flow in the extratropical middle atmosphere.

[9] No gravity wave drag parameterization is adopted in the model. Gravity waves in the GCM are spontaneously generated by topography, cumulus parameterization, hydrodynamic instability, and so on. The horizontal and vertical resolutions of the GCM are sufficient for representing the propagation and dissipation of gravity waves, except around the critical surface [*Lindzen and Fox-Rabinovitz*, 1989]. Total horizontal wavenumber (n) spectra for horizontal

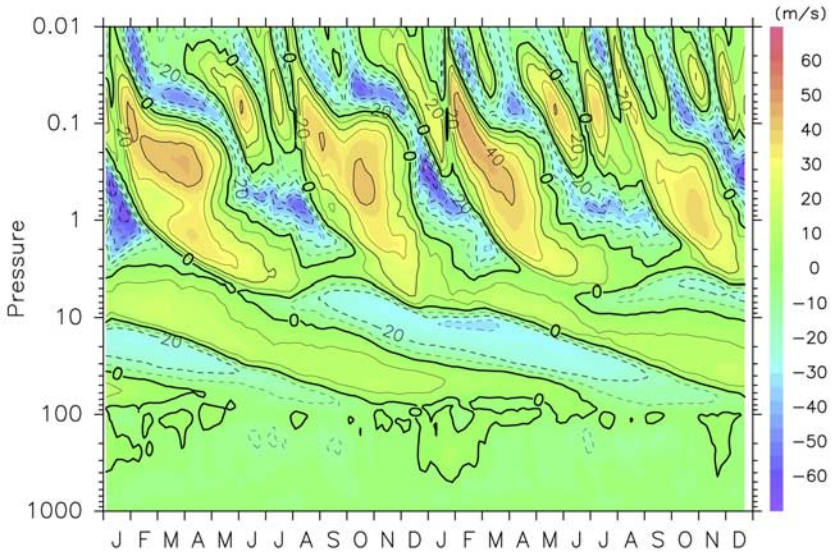

Figure 1. Time-pressure section of 6-day-mean and zonal-mean zonal wind at the equator. Contour intervals are 10 m s^{-1}.

kinetic energy of the divergent component corresponding to gravity waves have a slope of approximately $n^{-5/3}$ at n = 70–120, while it is shallower at n > 120 [*Watanabe et al.*, 2008]. This feature may indicate that the activity of gravity waves with n > 120 is overestimated in the GCM. On the other hand, orographic gravity waves in the GCM have realistic phase structure and temperature fluctuations similar to observations [*Watanabe et al.*, 2008]. The model has been integrated over three model years from initial conditions with a high level of spin-up. A companion paper by *Watanabe et al.* [2008] describes the resolved gravity waves and the experimental setup used in this study in greater detail.

[10] Figure 1 shows a time-pressure section of 6-day-mean and zonal-mean zonal wind at the equator. A downward propagation of easterly and westerly winds is observed between 3 and 80 hPa, which is similar to the quasi-biennial oscillation (QBO). Although the period of this QBO-like oscillation is about 15 months, which is shorter than the 28 months of the actual QBO, the magnitudes of its easterly and westerly maxima (i.e., ∼25 m s^{-1} and ∼15 m s^{-1} at 30 hPa, respectively) and its vertical and latitudinal widths are consistent with those of the actual QBO [*Baldwin et al.*, 2001]. The shorter period of the QBO-like oscillation than the actual QBO is probably due to upward momentum flux associated with the gravity waves larger than the observed, which will be discussed in detail by Kawatani et al. (to be submitted). Another oscillation of easterly and westerly winds corresponding to the stratopause semiannual oscillation (S-SAO) is observed around 1 hPa. Magnitudes of its easterly and westerly maxima are ∼35 m s^{-1} and ∼70 m s^{-1} for the first cycle, and ∼35 m s^{-1} and ∼50 m s^{-1} for the second cycle, respectively, which are consistent with the observations of S-SAO [*Garcia et al.*, 1997]. Although another semiannual oscillation out of phase with the S-SAO by 180 degrees is observed around 0.05 hPa, its features do not necessarily correspond to those of the mesospheric SAO, probably because of the effect of the model top.

3. Temperature Maximum and Meridional Circulation

[11] Figure 2 shows latitude-pressure sections of monthly-mean and zonal-mean temperature and zonal wind in June of the first model year and in January of the second model year. The stratopause, represented by a local temperature maximum in the vertical, is located around 1 hPa except near the winter pole, where it is located at 0.1–0.2 hPa [*Hitchman et al.*, 1989]. While the stratopause temperature generally decreases from the summer pole toward the winter midlatitudes (i.e., tropics, subtropics, and midlatitudes are hereafter referred to as 0–15, 15–30, and 30–45 degrees latitude regions, respectively, in this study), it is maximized at 20–30 degrees latitude in the winter hemisphere. Although the maximum temperature in the northern hemisphere is higher in December than in January, the monthly-mean temperature distribution in December is highly modulated because of a minor warming event in late December (not shown). Thus the temperature distribution in January, which is the most mirror-symmetric to that in June, is plotted here. Similar latitudinal temperature maxima are seen in a low-resolution (e.g., T32) GCM [*Beagley et al.*, 1997]. These latitudinal temperature maxima in the winter subtropics are accompanied by an easterly shear on the equatorward region, which satisfies the thermal wind balance. An easterly wind around the stratopause in the tropics is due to the easterly phase of the S-SAO. The easterly maximum associated with the S-SAO embedded in the mesospheric easterly jet is located at 0.5–0.8 hPa and 10–20 degrees latitude in the summer hemisphere. The westerly maximum of the polar-night jet (PNJ) is observed at 0.5–1 hPa and 45–60 degrees latitude in the winter hemisphere.

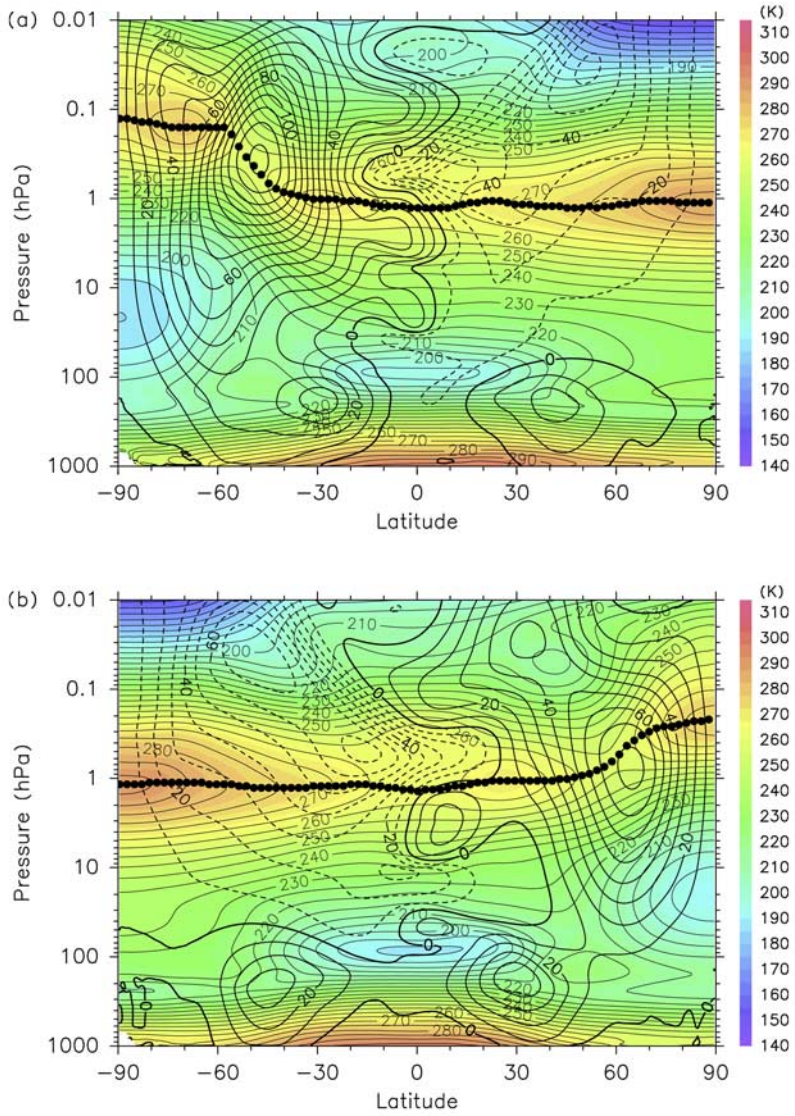

Figure 2. Latitude-pressure sections of monthly- and zonal-mean temperature (colors and thin contours) and zonal wind (thick contours) in (a) June of the first model year and (b) January of the second model year. Contour intervals are (thin) 5 K and (thick) 10 m s^{-1}. Solid circles represent the stratopause.

[12] For comparison, Figure 3 shows the latitude-pressure sections of monthly-mean and zonal-mean temperature and zonal wind in June and January of the 1986 CIRA (CIRA86) climatology based on satellite observations [*Fleming et al.*, 1990]. In CIRA86, the stratopause is located around 1 hPa, except around the winter pole in both June and January. The stratopause temperature has latitudinal maxima at 15–30 degrees latitude in the winter hemisphere, which is similar to that of the model. These latitudinal temperature maxima at the wintertime subtropical stratopause have been captured by other satellite observations as well [e.g., *Hitchman and Leovy*, 1986]. Thus it is considered that such a latitudinal temperature maximum is a robust feature at the subtropical stratopause in the winter hemisphere and is well simulated in the model used in this study.

[13] Figure 4 shows time-latitude sections of 6-day-mean and zonal-mean temperature at 1 hPa and zonal wind at 0.6 hPa, where the residual-mean meridional flow is strong, as shown in Figure 5, in the austral winter of the first model year and the boreal winter of the first/second model year. A pair of temperature maxima in the winter subtropics and minima in the tropics is observed from late May through August in the austral winter and from late December to early February in the boreal winter. However, periods and magnitudes of the stratopause temperature maxima and minima are rather different between the austral and boreal winters. The easterly maximum of S-SAO is observed in the summer subtropics (i.e., 10–15°N in Figure 4a and ~15°S in Figure 4b) slightly after the solstice, while the westerly of PNJ is strongest around 45 degrees latitude just before the winter solstice. The axis of PNJ shifts poleward after the winter solstice. These two jet streams (i.e., easterly of S-SAO and westerly of PNJ) create a strong anticyclonic shear between the equator and the axis of PNJ.

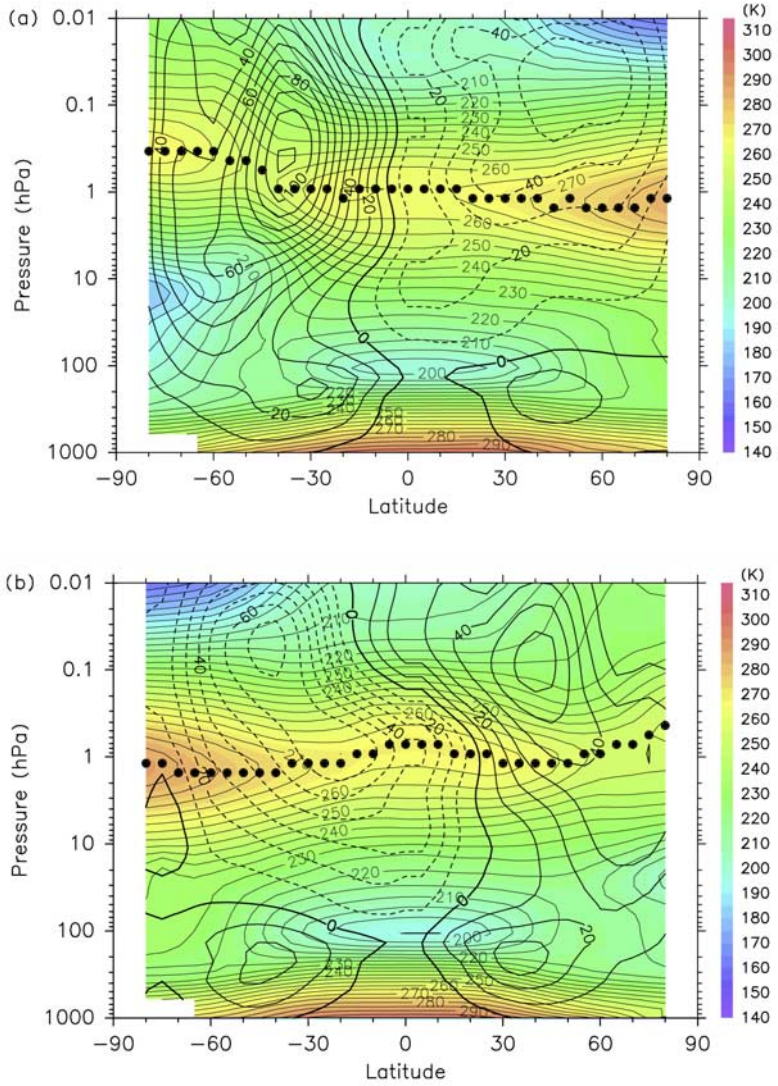

Figure 3. The same as Figure 2 but for CIRA86 climatology.

[14] These latitudinal temperature maxima at the wintertime subtropical stratopause do not appear in the radiative equilibrium temperature distribution [*Wehrbein and Leovy*, 1982]. Thus it is likely that the latitudinal temperature maxima are dynamically forced. Figure 5 shows meridional sections of monthly-mean and residual-mean meridional and vertical velocities in June of the first model year and January of the second model year. It is evident that the location of strong downwelling is almost in accordance with that of the temperature maximum at the wintertime subtropical stratopause. One exception is a slight equatorward shift of the temperature maximum because of a latitudinal gradient of radiative equilibrium temperature [cf., *Wehrbein and Leovy*, 1982]. This downwelling is part of the strong meridional circulation from summer tropics to winter subtropics passing above the stratopause. Although the meridional flow is from the summer toward the winter hemisphere throughout the stratosphere and mesosphere, its magnitude is maximized just above the stratopause in the tropics and winter subtropics. It is worth noting that upward and downward branches of the meridional circulation are observed above the downwelling and upwelling around the stratopause, respectively (i.e., reverse meridional circulation, see the studies by *Hitchman and Leovy* [1986] and *Delisi and Dunkerton* [1988]). Local temperature maxima around 0.5 hPa above the equator in Figure 2 are induced by downwelling of the reverse meridional circulation.

[15] Further evidence that the downwelling of the meridional circulation induces the latitudinal temperature maximum is given by time-latitude sections of zonal-mean temperature and residual-mean vertical velocity at 1 hPa shown in Figure 6. Since the stratopause air is adiabatically heated and cooled by upwelling and downwelling, the temperature maxima in the winter subtropics and minima in the tropics appear with a slight lag from the strong downwelling and upwelling events, respectively.

4. Meridional Circulation and Absolute Angular Momentum Distribution

[16] The transformed Eulerian-mean (TEM) zonal momentum equation is expressed as

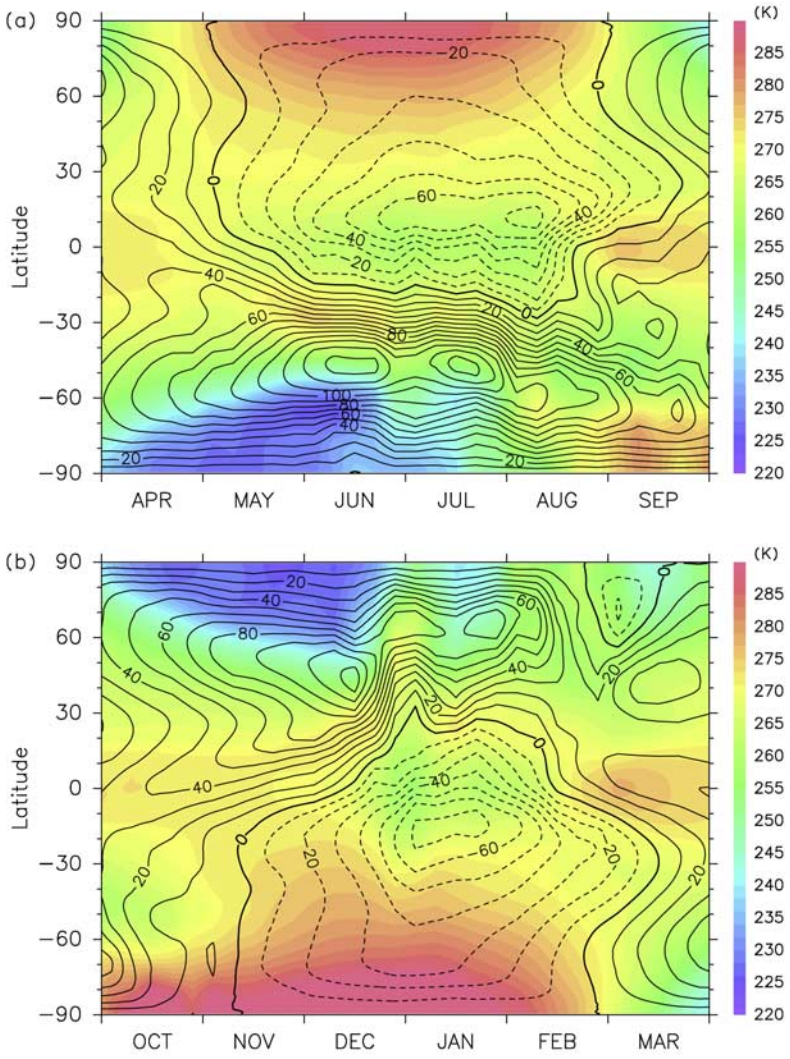

Figure 4. Time-latitude sections of 6-day-mean and zonal-mean temperature at 1 hPa (colors) and zonal wind at 0.6 hPa (thick contours) in (a) austral winter of the first model year and (b) boreal winter of the first/second model year. Contour intervals are 10 m s^{-1}.

$$\frac{\partial \mathrm{M}}{\partial t} + \frac{\bar{v}^*}{a}\frac{\partial \mathrm{M}}{\partial \phi} + \bar{w}^*\frac{\partial \mathrm{M}}{\partial z} = \rho_0^{-1}\nabla \cdot \mathbf{F} + \bar{X} a \cos\phi, \qquad (1)$$

where

$$\mathrm{M} \equiv a\cos\phi(\bar{u} + \Omega a \cos\phi) \qquad (2)$$

is the zonal-mean absolute angular momentum per unit mass, $\bar{u}$ the zonal-mean zonal wind, a the earth's radius, ϕ the latitude, Ω the angular velocity of earth's rotation, ρ_0 the basic density, $\nabla \cdot \mathbf{F}$ the Eliassen-Palm (E-P) flux divergence, $\bar{X}$ the zonal-mean unresolved mechanical forcing, and $\bar{v}^*$ and $\bar{w}^*$ the residual-mean meridional and vertical velocities, respectively [cf., *Andrews et al.*, 1987]. A contribution of the unresolved mechanical forcing is negligibly small compared to the E-P flux divergence throughout this paper. This equation indicates that the residual-mean meridional circulation ($\bar{v}^*$, $\bar{w}^*$) cannot cross the M contours without any torque given by the right-hand side of (1) in a steady-state condition. Since a radiative relaxation time is several days or shorter around the stratopause [*Wehrbein and Leovy*, 1982], a monthly-mean field approximately satisfies the steady-state assumption in the subtropics and midlatitudes. Although the steady-state assumption is not valid in the tropics because of the slow relaxation toward the radiative equilibrium [*Scott and Haynes*, 1998], the first term on the left-hand side of (1) is relatively small (i.e., $\sim$ one third in the tropics and $\sim$ one tenth in the winter subtropics) compared to the advective and E-P flux divergence terms of (1) on a monthly-mean basis (not shown). Thus the meridional circulation around the stratopause primarily depends on the distributions of absolute angular momentum and E-P flux divergence.

[17] Figure 7 shows latitude-pressure sections of monthly-mean and zonal-mean absolute angular momentum (M), meridional circulation ($\bar{v}^*$, $\bar{w}^*$), and zonal wind acceleration force associated with the E-P flux divergence ($\equiv(\rho_0 a\cos\phi)^{-1}\nabla \cdot \mathbf{F}$) in June of the first model year and January of the second model year. A strong meridional circulation from

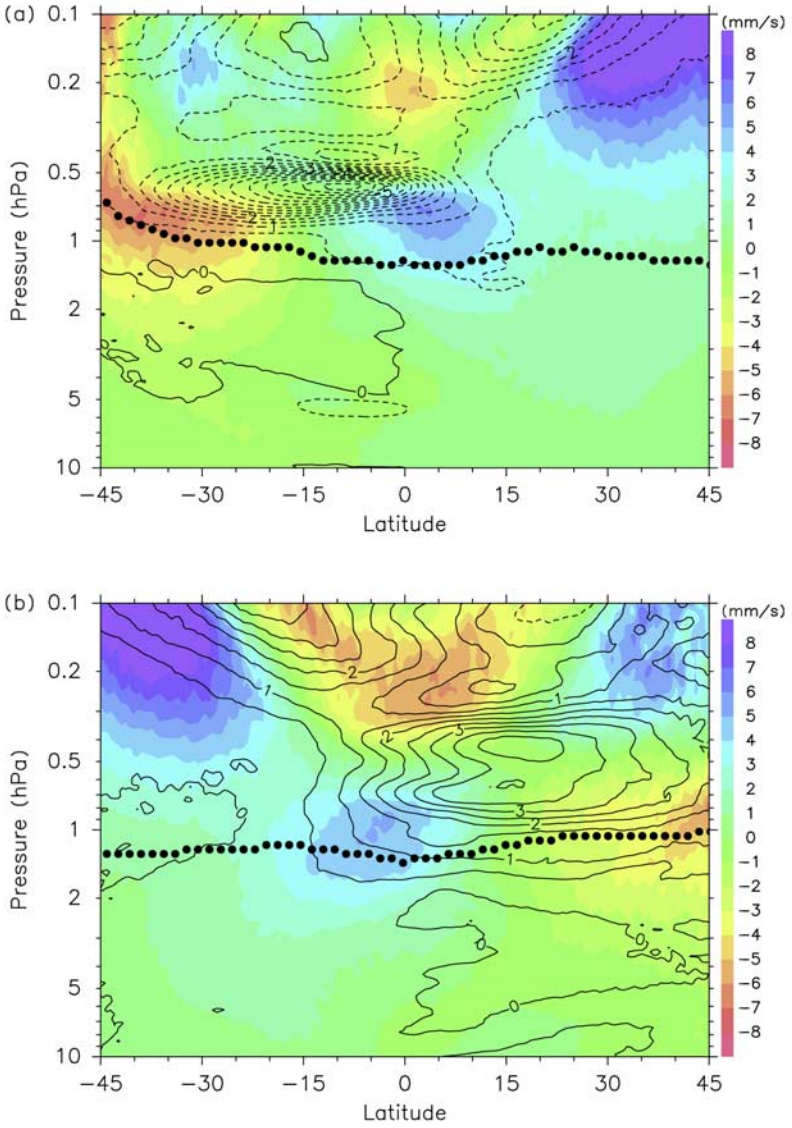

Figure 5. Latitude-pressure sections of monthly- and residual-mean meridional (contours) and vertical velocities (colors) in (a) June and (b) January. Contour intervals are 0.5 m s^{-1}. Solid circles represent the stratopause.

summer tropics to winter subtropics passing above the stratopause can be seen both in June and January (see also Figure 5). Momentum advection due to the meridional flow is dominant in (1) in the subtropics, while it is comparable to or weaker than that due to the vertical flow in the tropics (not shown). Dividing the meridional flow into tropical and subtropical parts helps us to understand the underlying mechanism.

4.1. Winter Subtropics

[18] The strong poleward flow in the winter subtropics is associated with nearly vertically aligned M contours (Figure 7) so that the residual-mean meridional velocity is approximated by

$$\bar{v}^* \approx -\frac{(\rho_0 a\cos\phi)^{-1}\nabla\cdot\mathbf{F}}{f-(a\cos\phi)^{-1}(\bar{u}\cos\phi)_\phi} \qquad (3)$$

in the steady-state limit, where f is the Coriolis parameter. The denominator of (3) is a zonal-mean absolute vorticity, which is equivalent to the latitudinal gradient of M. It follows that the residual-mean meridional velocity is approximated by the E-P flux convergence divided by the zonal-mean absolute vorticity. Figure 8 shows time variations of 6-day-mean and residual-mean meridional velocity, zonal-mean absolute vorticity, and zonal wind acceleration force associated with the E-P flux divergence averaged over 15–30°S and 15–30°N at 0.6 hPa, where the residual-mean meridional velocity is large in the austral and boreal winters, respectively. The E-P flux convergence has a large short-term (i.e., weekly timescale) variability, which is in accordance with the strength of the residual-mean meridional velocity. On the other hand, the seasonal variation of the residual-mean meridional velocity is likely due to that of the absolute vorticity, as well as that of the E-P flux convergence.

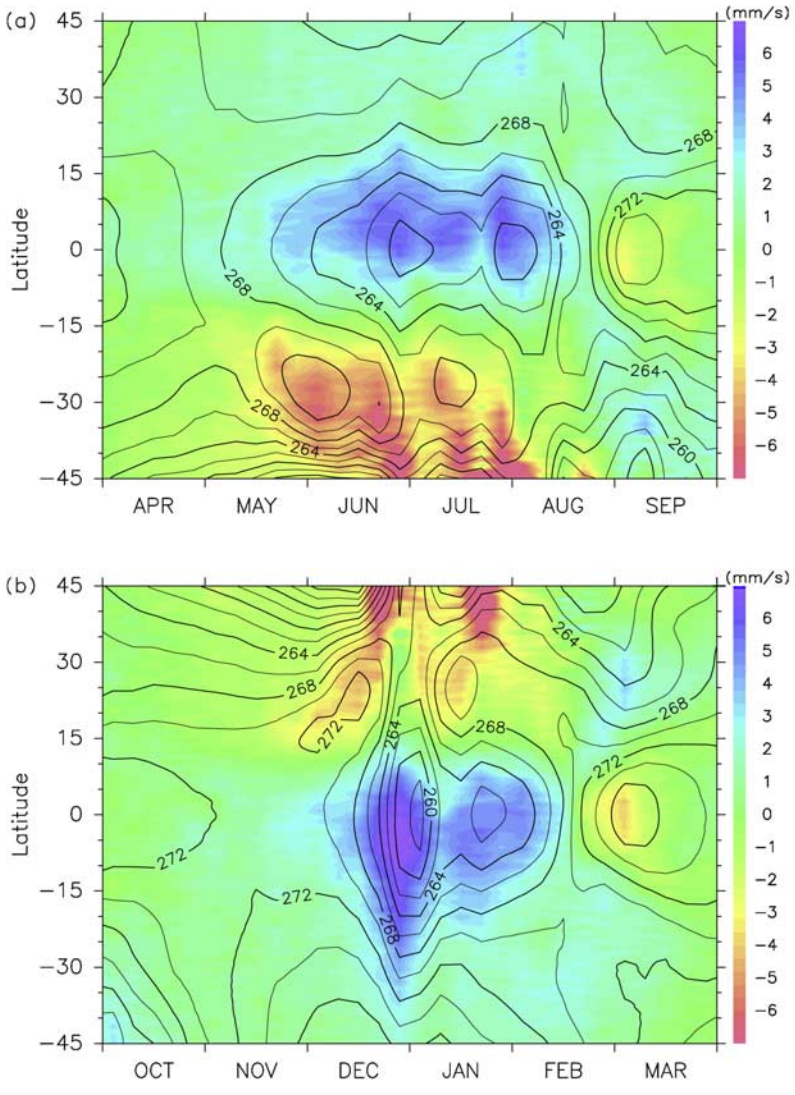

Figure 6. Time-latitude sections of 6-day-mean and zonal-mean temperature (contours) and residual-mean vertical velocity (colors) at 1 hPa in (a) austral winter and (b) boreal winter. Contour intervals are 2 K.

[19] The time variation of the absolute vorticity in Figure 8 is nearly proportional to that of the zonal wind difference between 15 and 30 degrees latitudes in the winter hemisphere. Since the location and strength of the easterly phase of S-SAO and the westerly of polar-night jet (PNJ) have large seasonal variations as discussed in section 3, the zonal wind difference between 15 and 30 degrees latitudes in the winter hemisphere also varies seasonally. This fact suggests that the seasonal variation of meridional flow in the winter subtropics above the stratopause is significantly affected by the seasonal variation of zonal wind structure associated with the S-SAO and PNJ.

4.2. Tropics

[20] Solid circles in Figure 7 represent the latitude of maximum absolute angular momentum at each pressure level (hereafter, referred to as "Mmax"). Because of the rotation of the earth and the westerly and easterly jets in the winter and summer hemispheres, respectively, Mmax is shifted off the equator toward the winter hemisphere by 0–5 degrees latitude. Since the latitudinal gradient of M (i.e., absolute vorticity) is zero at Mmax, the M contour is horizontal at Mmax and extends from the winter tropics toward the winter subtropics and summer tropics. When the M value at Mmax is small (i.e., around 0.6 hPa), the winter subtropics and summer tropics are connected by the same M contour, as shown in Figure 7. The residual-mean meridional flow at Mmax is driven not by a local torque because of the zero absolute vorticity there, but is induced to satisfy mass continuity along the M contour. When the M value at Mmax is small, a strong meridional flow must be induced at Mmax along the M contour to satisfy mass continuity with strong poleward flow in the winter subtropics.

[21] Figure 9 shows time-pressure sections of 6-day-mean and zonal-mean absolute angular momentum and residual-mean meridional velocity at the latitudes of Mmax during austral and boreal winters. The strong meridional flow from the summer to winter hemisphere is in accordance with the

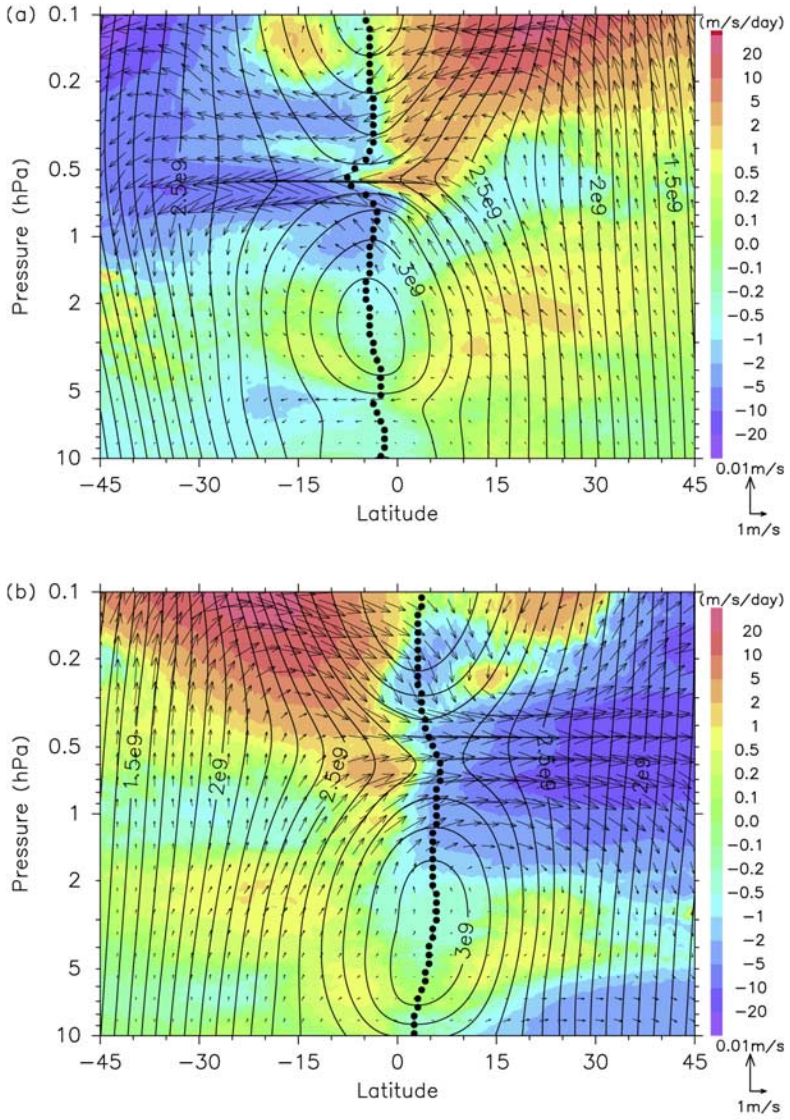

Figure 7. Latitude-pressure sections of monthly- and zonal-mean absolute angular momentum (contours), zonal wind acceleration force associated with the E-P flux divergence (colors), and residual-mean circulation (vectors) in (a) June and (b) January. Contour intervals are 10^8 m^2 s^{-1}. Solid circles represent the latitude of maximum absolute angular momentum at each pressure level (Mmax).

small absolute angular momentum at Mmax. On the other hand, the E-P flux divergence in the tropics does not necessarily change its sign at Mmax (Figure 7), in which case the wave-driven flow is not in the same direction as the cross-equatorial meridional flow around Mmax. These facts suggest that the strong cross-equatorial flow is not driven by the local wave-induced torque, but is induced along the nearly horizontally aligned M contours passing through the easterly phase of S-SAO.

[22] The short-term variability of the residual-mean meridional velocity at Mmax is probably due to that in the winter subtropics because their short-term variabilities are in strong accordance (see Figure 8). On the other hand, there can be seen a large difference between austral and boreal winters in the downward propagation of the small absolute angular momentum at Mmax corresponding to the easterly phase of S-SAO and that of the strong meridional flow at Mmax. Such a difference of the descent of the S-SAO easterly is attributable to the difference of zonal wind acceleration mechanism in the tropics between the austral and boreal winters. While the local E-P flux divergence/convergence mainly induces the downward propagation of S-SAO easterly in austral winter, as shown in the next paragraph, the momentum advection is more important than the local E-P flux divergence/convergence for the downward propagation of S-SAO easterly in the boreal winter (not shown).

[23] While the easterly phase of S-SAO with a small absolute angular momentum in the tropics acts as a corridor for the meridional circulation across the equator, momentum advection due to the meridional circulation is considered to play a significant role for driving the easterly phase of S-SAO [*Holton and Wehrbein*, 1980; *Delisi and Dunkerton*, 1988]. In order to clarify the causality between the easterly

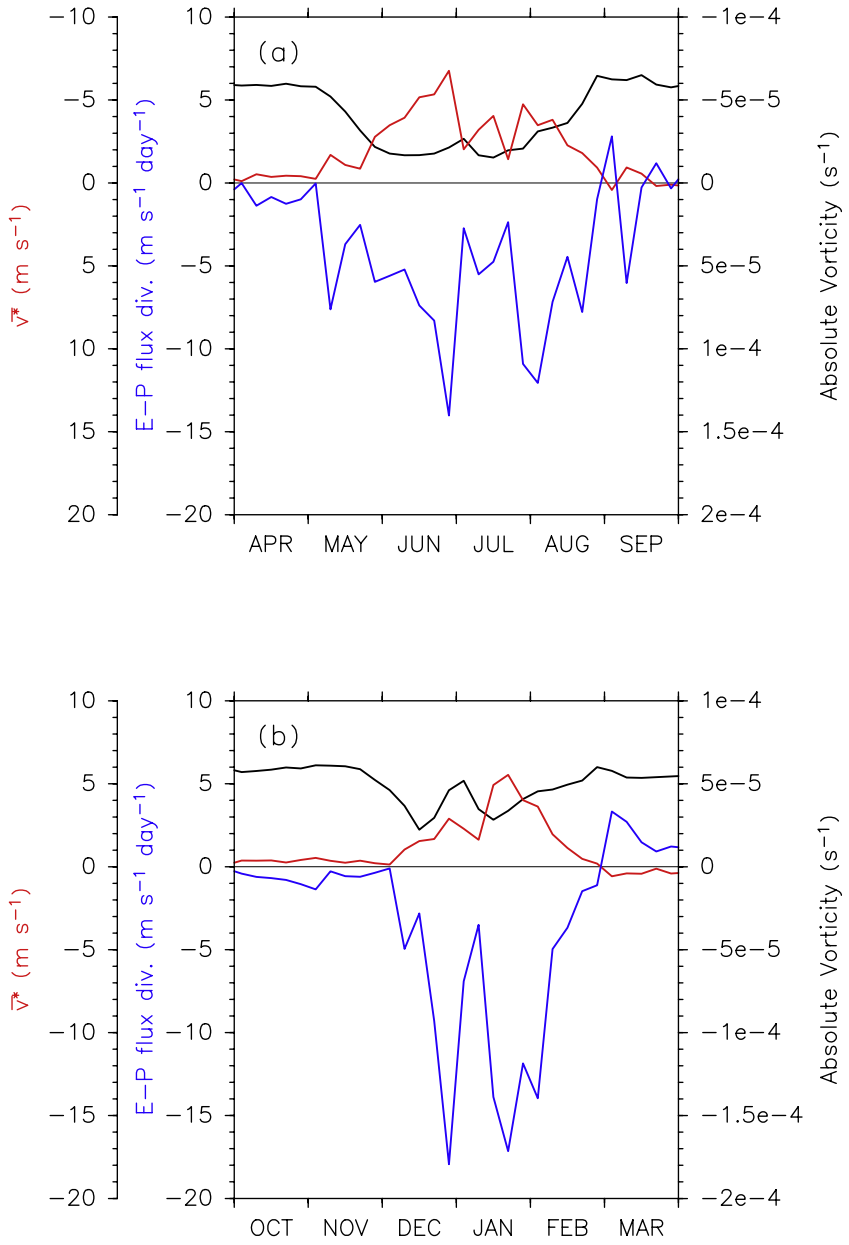

Figure 8. Time variations of 6-day-mean and residual-mean meridional velocity (red), zonal-mean absolute vorticity (black), and zonal wind acceleration force associated with the E-P flux divergence (blue) averaged over (a) 15–30°S and (b) 15–30°N at 0.6 hPa in austral and boreal winters, respectively. Vertical axes for residual-mean meridional velocity and zonal-mean absolute vorticity are reversed in Figure 8a.

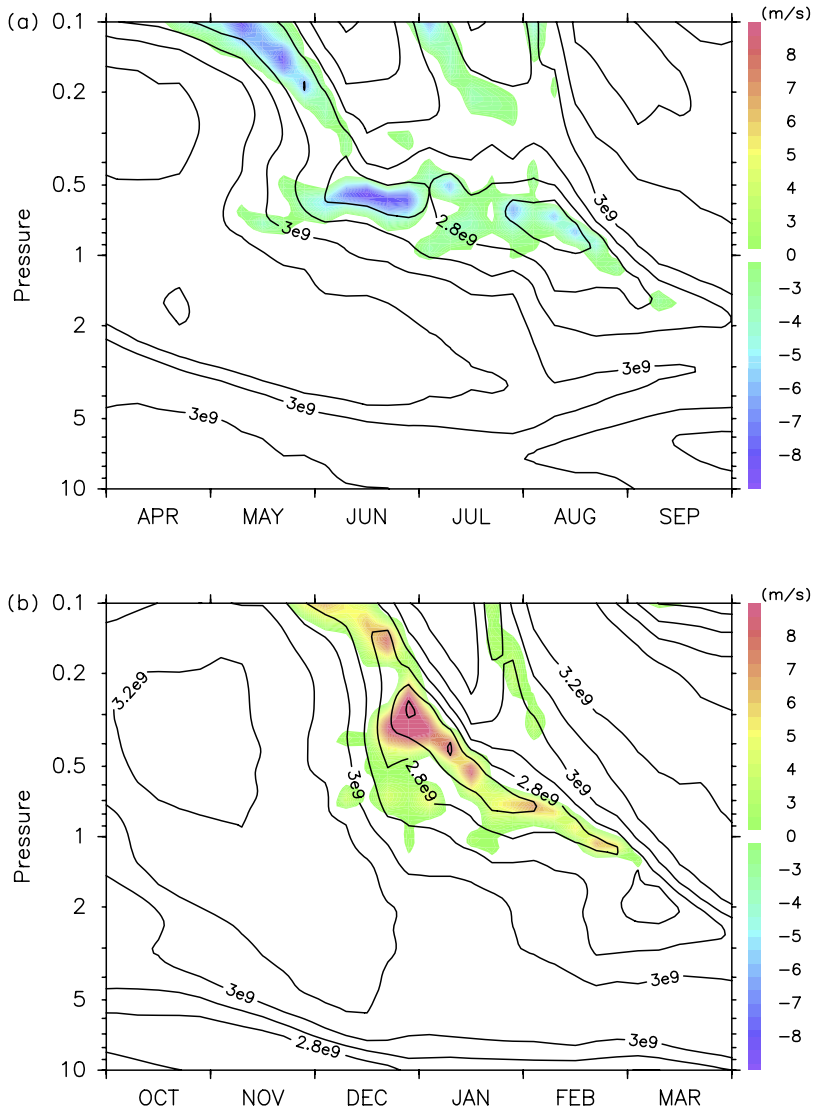

Figure 9. Time-pressure sections of (contours) maximum of 6-day-mean and zonal-mean absolute angular momentum at each pressure level (i.e., the M value at Mmax) and (colors) residual-mean meridional velocity at Mmax in (a) austral winter and (b) boreal winter. Contour intervals are 10^8 m^2 s^{-1}.

phase of S-SAO and the cross-equatorial meridional circulation, a time-pressure section of each term in the zonal momentum balance (cf., (1)) averaged over 10°S–10°N in austral winter is examined (shown in Figure 10). A pair of downward-propagating positive and negative signals of the zonal wind acceleration in May (Figure 10a) represent the downward propagation of the easterly phase of S-SAO. The positive and negative zonal wind acceleration above 0.3 hPa is due primarily to the local E-P flux divergence and convergence, respectively (Figure 10c). In contrast, the easterly acceleration (i.e., negative signal in Figure 10a) at 0.4–0.8 hPa in May is due primarily to the momentum advection (Figure 10b).

[24] The E-P flux divergence/convergence and momentum advection nearly cancel each other in June and July at 0.4–1 hPa, resulting in a small time variation of the easterly maximum of S-SAO. The westerly (i.e., positive) momentum advection below 0.6 hPa (Figure 10b) is due primarily to the vertical flow in spite of the strong cross-equatorial flow there. The small horizontal gradient of M associated with the easterly phase of S-SAO enables the strong cross-equatorial flow to exist without inducing a large momentum advection. Thus it is found that the causality between the easterly phase of S-SAO and the cross-equatorial meridional circulation depends on the phase of S-SAO. During the development phase of the easterly of S-SAO (i.e., May), the meridional circulation plays a primary role in the acceleration of the easterly of S-SAO through the advection of easterly momentum. During the mature phase of the easterly of S-SAO (i.e., June and July), the strong cross-equatorial flow is along the nearly horizontally aligned M contours rather than across them, and the easterly phase of S-SAO acts as a corridor for the cross-equatorial flow.

5. Waves Responsible for E-P Flux Convergence

[25] As shown in the previous section, the large E-P flux convergence above the stratopause in the winter subtropics

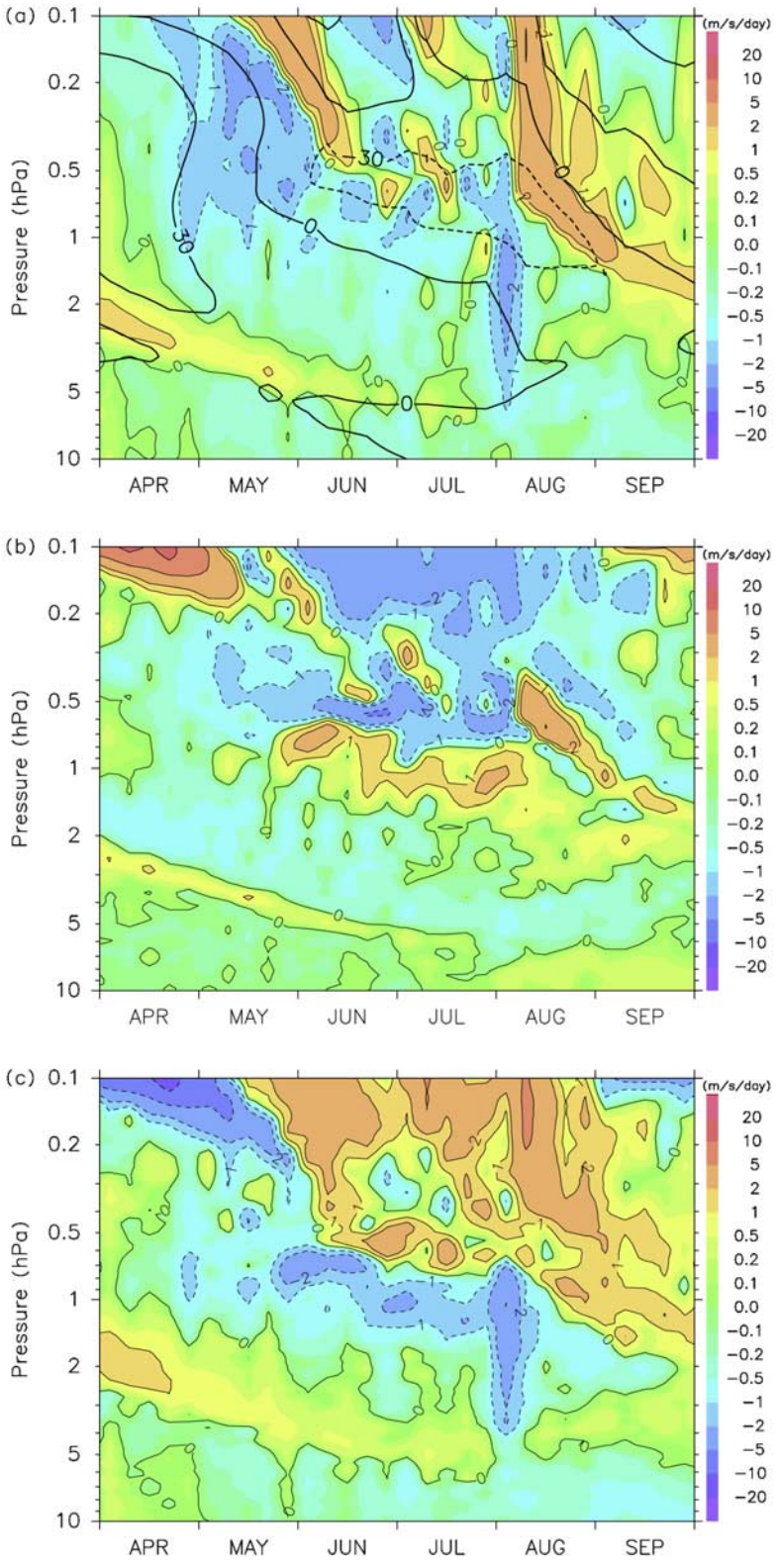

Figure 10. Time-pressure sections of 6-day-mean and zonal-mean (a) zonal wind acceleration, (b) and zonal wind acceleration force due to the momentum advection, and (c) zonal wind acceleration force due to the E-P flux divergence averaged over 10°S–10°N in austral winter.

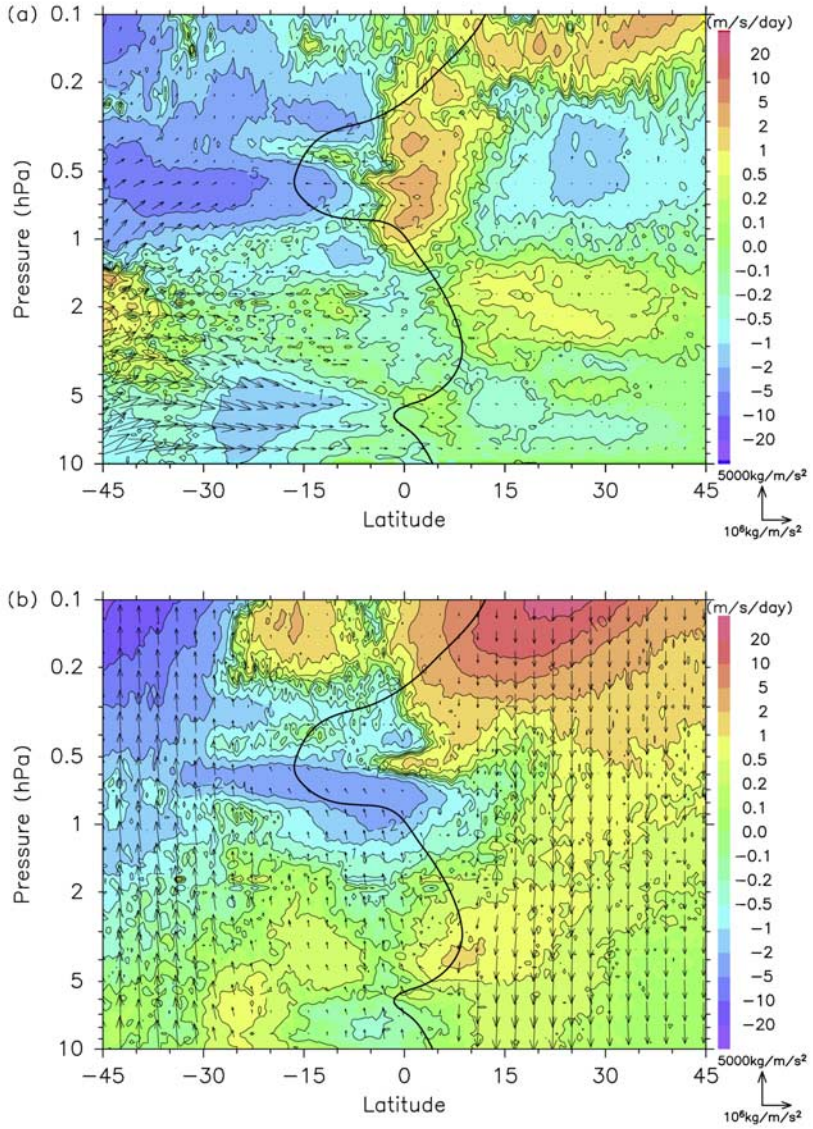

Figure 11. Latitude-pressure sections of monthly-mean E-P flux (vector) and zonal wind acceleration force associated with the E-P flux divergence (colors and contours) due to waves with (a) zonal wavenumbers 1–3 and (b) zonal wavenumber larger than 3 in June. Thick solid lines represent contours of 0 m s^{-1} zonal-mean zonal wind.

contributes to driving the strong poleward flow. In order to examine what waves are responsible for the large E-P flux convergence, meridional sections of E-P flux and its divergence due to waves with zonal wavenumbers of 1–3 and larger than 3 in June of the first model year are presented in Figure 11. An upward and equatorward E-P flux due to zonal wavenumbers of 1–3 approach the zero wind line of zonal-mean zonal wind above the subtropical stratopause in the winter hemisphere and induces a large convergence a little before the zero wind line (Figure 11a). This E-P flux is due primarily to the extratropical planetary waves with a zonal wavenumber 2 and a zonal phase velocity of 15–20 m s^{-1} (not shown). The zero wind line located in the winter subtropics is due to the easterly phase of S-SAO.

[26] At the same time, a cross-equatorial E-P flux from the summer to winter hemisphere due to zonal wavenumbers of 1–3 also contributes to its convergence in the winter subtropics and divergence in the summer tropics around 0.6 hPa. The E-P flux computed from 4-day lowpass-filtered data still has large convergence in the winter subtropics and divergence in the summer tropics (not shown) so that this cross-equatorial E-P flux is not due to 2-day waves dominant around the summertime subtropical stratopause [*Limpasuvan and Leovy*, 1995; *Orsolini et al.*, 1997]. Since this cross-equatorial E-P flux is largest on 29 June, horizontal and vertical cross sections of the daily-mean temperature with zonal wavenumbers 1–3 on 29 June are shown in Figure 12. The temperature anomaly with zonal wavenumbers 1–2 is observed in the tropics, which has little phase shift with latitude (Figure 12a). It has a vertically stacked structure with a vertical scale of several kilometers (Figure 12b). This temperature anomaly is quasi-stationary. These features are consistent with the character-

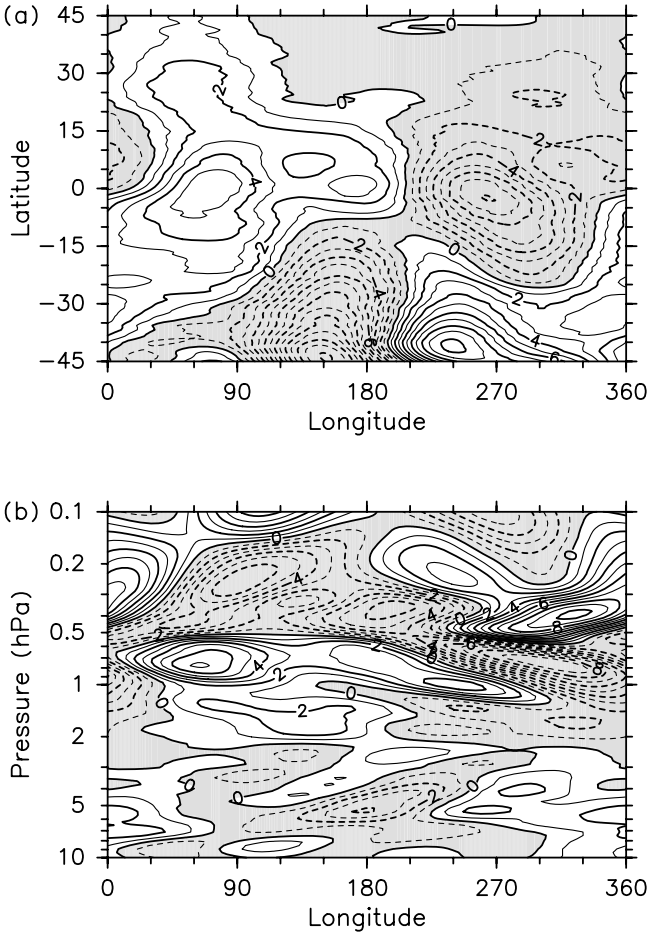

Figure 12. Cross-sections of (a) longitude-latitude at 0.6 hPa and (b) longitude-pressure at the equator of daily-mean temperature with zonal wavenumbers 1–3 on 29 June of the first model year. Negative values are shaded. Contour intervals are 1 K.

istics of asymmetric inertial instability [*Hitchman et al.*, 1987].

[27] On the other hand, an upward E-P flux due to zonal wavenumbers larger than 3 contributes to the E-P flux convergence just below the easterly phase of S-SAO in the winter tropics. This upward E-P flux is likely due to equatorial and small-scale gravity waves with a westward phase velocity excited in the tropical lower atmosphere. These waves are filtered out in the easterly shear of S-SAO and induce the E-P flux convergence there. This E-P flux convergence contributes to maintaining the momentum balance around the tropical stratopause, as shown in section 4. Evaluating relative contributions of equatorial and small-scale gravity waves will be performed by Kawatani et al. (to be submitted) using an equatorial wave filter.

6. Concluding Remarks

[28] A wintertime temperature maximum at the subtropical stratopause can be seen in the CIRA86 climatology, a feature which has not drawn much attention in previous studies. A similar wintertime temperature maximum at the subtropical stratopause was well simulated using a T213L256 GCM and examined in detail. The stratopause temperature is latitudinally maximized in the winter subtropics because of a strong downwelling of the meridional circulation from the summer tropics to the winter subtropics passing above the stratopause.

[29] The mechanism driving the strong meridional flow of the meridional circulation differs between the tropics and winter subtropics. The strong poleward flow in the winter subtropics with nearly vertically aligned contours of absolute angular momentum (M) is attributable to the large Eliassen-Palm (E-P) flux convergence and a small magnitude of the absolute vorticity there. The large E-P flux convergence is due to the extratropical planetary waves and asymmetric inertial instability with a large short-term (i.e., weekly timescale) variability. The small magnitude of the absolute vorticity in the winter subtropics is due to the strong anticyclonic shear associated with the easterly phase of the stratopause semiannual oscillation (S-SAO) and the westerly of the polar-night jet (PNJ). The seasonal variations of the S-SAO and PNJ (i.e., their strength and latitude) partly contribute to that of the meridional flow in the winter subtropics.

[30] On the other hand, the strong cross-equatorial meridional flow just above the tropical stratopause with nearly horizontally aligned M contours is induced along the M contour to satisfy the mass continuity with the strong poleward flow in the winter subtropics. A strong cross-equatorial flow can exist in the easterly phase of S-SAO, where the M contours are nearly horizontal. While the short-term variability of the cross-equatorial meridional flow is attributable to that of the meridional flow in the winter subtropics, its seasonal variation is mainly controlled by that of the S-SAO (i.e., its strength and height). A formation mechanism for the wintertime temperature maximum at the subtropical stratopause is schematically summarized in Figure 13.

[31] The cross-equatorial meridional circulation can drive the easterly phase of S-SAO through the advection of easterly momentum. The causality between the easterly phase of S-SAO and the cross-equatorial meridional circulation depends on the phase of S-SAO. During the development phase of the easterly of S-SAO, advection of easterly momentum due to the meridional circulation is the primary acceleration mechanism for the easterly phase of S-SAO. During the mature phase of the easterly of S-SAO, the momentum advection and the E-P flux divergence/convergence nearly cancel each other, and the easterly phase of S-SAO acts as a corridor for the cross-equatorial meridional circulation.

[32] As shown in section 4, the latitudinal maximum of absolute angular momentum at each pressure level (Mmax) is shifted off the equator toward the winter hemisphere by about 5 degrees. The latitude region between the equator and Mmax satisfies the necessary condition for the symmetric inertial instability [*Dunkerton*, 1982]. However, a contribution of the symmetric inertial instability to the monthly-mean meridional flow in the tropics is considered to be small because a signature of the symmetric inertial instability is not clearly seen in the zonal-mean meridional flow around the equator, even on a daily-mean basis (not

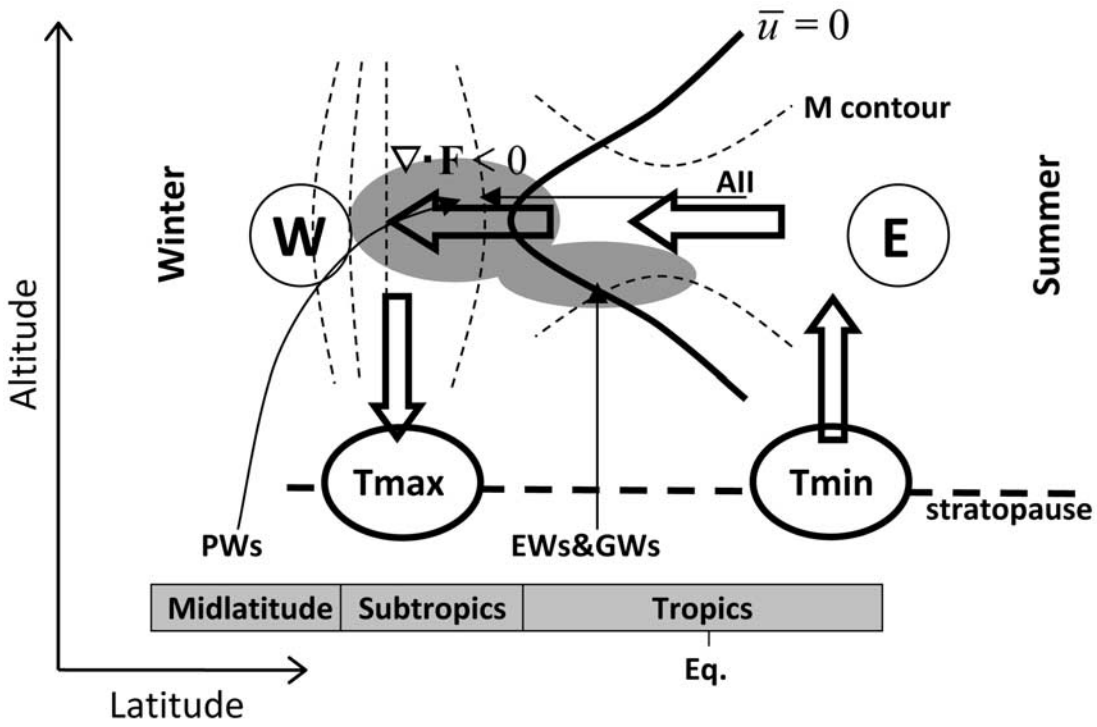

Figure 13. A schematic view of the formation mechanism of wintertime temperature maximum at the subtropical stratopause. Circled W and E denote the polar-night jet and the mesospheric easterly jet, respectively; dashed contours, the absolute angular momentum (M); shaded ellipses, the E-P flux convergence regions; Tmax and Tmin the temperature maximum and minimum, respectively; box and thin arrows, the meridional circulation and the E-P flux, respectively, of planetary (PWs), equatorial (EWs), and gravity waves (GWs), and asymmetric inertial instability (AII).

shown). On the other hand, the symmetric inertial instability can contribute to the formation of the easterly phase of the S-SAO, which is a region conducive to cross-equatorial flow through the homogenization of absolute angular momentum in the winter tropics. This topic is beyond the scope of this paper and will be dealt with in a future study.

[33] **Acknowledgments.** The authors thank three anonymous reviewers for their helpful comments and suggestions. This work is a contribution to the Innovative Program of Climate Change Projection for the 21st Century, MEXT, Japan. The simulation was conducted using the Earth Simulator. The GFD-DENNOU Library was used for drawing the figures. This work was supported by Grant-in-Aid for Scientific Research 19204047 (PI: Kaoru Sato) of the Ministry of Education, Culture, Sports, Science and Technology, Japan.

References

Alexander, M. J. (1998), Interpretations of observed climatological patterns in stratospheric gravity wave variance, *J. Geophys. Res.*, *103*, 8627–8640.

Allen, S. J., and R. A. Vincent (1995), Gravity wave activity in the lower atmosphere: Seasonal and latitudinal variations, *J. Geophys. Res.*, *100*, 1327–1350.

Andrews, D. G., J. R. Holton, and C. B. Leovy (1987), *Middle Atmosphere Dynamics*, 489 pp, Academic Press, San Diego, Calif.

Baldwin, M. P., et al. (2001), The quasi-biennial oscillation, *Rev. Geophys.*, *39*, 179–229.

Beagley, S. R., J. de Grandpré, J. N. Koshyk, N. A. McFarlane, and T. G. Shepherd (1997), Radiative-dynamical climatology of the first-generation Canadian middle atmosphere model, *Atmos. Ocean*, *35*, 293–331.

Blum, U., K. H. Fricke, G. Baumgarten, and A. Schöch (2004), Simultaneous lidar observations of temperatures and waves in the polar middle atmosphere on the east and west side of the Scandinavian mountains: A case study on 19/20 January 2003, *Atmos. Chem. Phys.*, *4*, 809–816.

Delisi, D. P., and T. J. Dunkerton (1988), Seasonal variation of the semiannual oscillation, *J. Atmos. Sci.*, *45*, 2772–2787.

Duck, T. J., J. A. Whiteway, and A. I. Carswell (2001), The gravity wave-arctic stratospheric vortex interaction, *J. Atmos. Sci.*, *58*, 3581–3596.

Dunkerton, T. J. (1982), On the inertial stability of the equatorial middle atmosphere, *J. Atmos. Sci.*, *38*, 2354–2364.

Dunkerton, T. J. (1989), Nonlinear Hadley circulation driven by asymmetric differential heating, *J. Atmos. Sci.*, *46*, 956–974.

Dunkerton, T. J. (1991), Nonlinear propagation of zonal winds in an atmosphere with Newtonian cooling and equatorial wavedriving, *J. Atmos. Sci.*, *48*, 236–263.

Eckermann, S. D., and P. Preusse (1999), Global measurements of stratospheric mountain waves from space, *Science*, *286*, 1534–1537.

Eliassen, A. (1951), Slow thermally or frictionally controlled meridional circulation in a circular vortex, *Astrophys. Norv.*, *5*, 19–60.

Ern, M., P. Preusse, M. J. Alexander, and C. D. Warner (2004), Absolute values of gravity wave momentum flux derived from satellite data, *J. Geophys. Res.*, *109*, D20103, doi:10.1029/2004JD004752.

Fetzer, E. J., and J. C. Gille (1994), Gravity wave variance in LIMS temperature. part I: Variability and comparison with background winds, *J. Atmos. Sci.*, *51*, 2461–2483.

Fleming, E. L., S. Chandra, J. J. Barnett, and M. Corney (1990), Zonal mean temperature, pressure, zonal wind, and geopotential height as functions of latitude, COSPAR International Reference Atmosphere: 1986. part II: Middle atmosphere models, *Adv. Space Res.*, *10*, 11–59.

Garcia, R. R. (1987), On the mean meridional circulation of the middle atmosphere, *J. Atmos. Sci.*, *44*, 3599–3609.

Garcia, R. R., T. J. Dunkerton, R. S. Lieberman, and R. A. Vincent (1997), Climatology of the semiannual oscillation of the tropical middle atmosphere, *J. Geophys. Res.*, *102*, 26,019–26,032.

Haynes, P. H., C. J. Marks, M. E. McIntyre, T. G. Shepherd, and K. P. Shine (1991), On the "downward control" of extratropical diabatic circulations by eddy-induced mean zonal forces, *J. Atmos. Sci.*, *48*, 651–678.

Hirota, I. (1978), Equatorial waves in the upper stratosphere and mesosphere in relation to semi-annual oscillation of the zonal wind, *J. Atmos. Sci.*, *35*, 714–722.

Hirota, I. (1980), Observational evidence of the semiannual oscillation in the tropical middle atmosphere: A review, *Pure Appl. Geophys.*, *118*, 217–238.

Hitchman, M. H., and C. B. Leovy (1986), Evolution of the zonal mean state in the equatorial middle atmosphere during October 1978–May 1979, *J. Atmos. Sci.*, *43*, 3159–3176.

Hitchman, M. H., C. B. Leovy, J. C. Gille, and P. L. Bailey (1987), Quasi-stationary zonally asymmetric circulations in the equatorial lower mesosphere, *J. Atmos. Sci.*, *44*, 2219–2236.

Hitchman, M. H., and C. B. Leovy (1988), Estimation of Kelvin wave contribution to the semiannual oscillation, *J. Atmos. Sci.*, *45*, 1462–1475.

Hitchman, M. H., J. C. Gille, C. D. Rogers, and G. Brasseur (1989), The separated polar winter stratopause: A gravity wave driven climatological feature, *J. Atmos. Sci.*, *46*, 410–422.

Holton, J. R., and W. M. Wehrbein (1980), The role of planetary waves in the annual cycle of the zonal mean circulation of the middle atmosphere, *J. Atmos. Sci.*, *37*, 1968–1983.

Kawatani, Y., S. K. Dhaka, M. Takahashi, and T. Tsuda (2003), Large potential energy of gravity waves over a smooth surface with little convection: Simulation and observation, *Geophys. Res. Lett.*, *30*(8), 1438, doi:10.1029/2003GL016960.

Kawatani, Y., M. Takahashi, and T. Tokioka (2004), Gravity waves around the subtropical jet of the southern winter in an atmospheric general circulation model, *Geophys. Res. Lett.*, *31*, L22109, doi:10.1029/2004GL020794.

Kawatani, Y., K. Tsuji, and M. Takahashi (2005), Zonally non-uniform distribution of equatorial gravity waves in an atmospheric general circulation model, *Geophys. Res. Lett.*, *32*, L23815, doi:10.1029/2005GL024068.

Kitamura, Y., and I. Hirota (1989), Small-scale disturbances in the lower stratosphere revealed by daily Rawin Sonde observations, *J. Meteorol. Soc. Jpn.*, *67*, 817–831.

K-1 Model Developers (2004), K-1 coupled model (MIROC) description, *K-1 Technical Report*, 1, edited by H. Hasumi and S. Emori, 34 pp, Center for Climate System Research, Univ. of Tokyo, Japan.

Limpasuvan, V., and C. B. Leovy (1995), Observation of the two-day wave near the southern summer stratopause, *Geophys. Res. Lett.*, *22*, 2385–2388.

Lindzen, R. S., and M. Fox-Rabinovitz (1989), Consistent vertical and horizontal resolution, *Mon. Weather Rev.*, *117*, 2575–2583.

Müller, K. M., U. Langematz, and S. Pawson (1997), The stratopause semiannual oscillation in the Berlin troposphere-stratosphere-mesosphere GCM, *J. Atmos. Sci.*, *54*, 2749–2759.

Nozawa, T., T. Nagashima, T. Ogura, T. Yokohata, N. Okada, and H. Shiogama (2007), Climate change simulations with a coupled ocean-atmosphere GCM called the model for interdisciplinary research on climate: MIROC, *CGER's Supercomputer Monograph Report Vol. 12*, 79 pp, Center for Global Environmental Research, NIES, Tsukuba, Japan.

Orsolini, Y. J., V. Limpasuvan, and C. B. Leovy (1997), The tropical stratopause in the UKMO stratospheric analyses: Evidence for a 2-day wave and inertial circulations, *Q. J. R. Meteorol. Soc.*, *123*, 1707–1724.

Pawson, S., et al. (2000), The GCM-Reality Intercomparison Project for SPARC (GRIPS): Scientific issues and initial results, *Bull. Am. Meteorol. Soc.*, *81*, 781–796.

Plumb, R. A., and J. Eluszkiewics (1999), The Brewer-Dobson circulation: Dynamics of the tropical upwelling, *J. Atmos. Sci.*, *56*, 868–690.

Ray, E. A., M. J. Alexander, and J. R. Holton (1998), An analysis of the structure and forcing of the equatorial semiannual oscillation in zonal wind, *J. Geophys. Res.*, *103*, 1759–1774.

Reed, R. J. (1962), Some features of the annual temperature regime in the tropical stratosphere, *Mon. Weather Rev.*, *90*, 211–215.

Reed, R. J. (1966), Zonal wind behavior in the equatorial stratosphere and lower mesosphere, *J. Geophys. Res.*, *71*, 4223–4233.

Sato, K. (1994), A statistical study of the structure, saturation and sources of inertio-gravity waves in the lower stratosphere observed with the MU radar, *J. Atmos. Terr. Phys.*, *56*, 755–774.

Sato, K., and T. J. Dunkerton (1997), Estimates of momentum flux associated with equatorial Kelvin and gravity waves, *J. Geophys. Res.*, *102*, 26,247–26,261.

Sato, K., T. Kumakura, and M. Takahashi (1999), Gravity waves appearing in a high-resolution GCM simulation, *J. Atmos. Sci.*, *56*, 1005–1018.

Sato, K., M. Yamamori, S. Ogino, N. Takahashi, Y. Tomikawa, and T. Yamanouchi (2003), A meridional scan of the stratospheric gravity wave field over the ocean in 2001 (MeSSO2001), *J. Geophys. Res.*, *108*(D16), 4491, doi:10.1029/2002JD003219.

Scott, R. K., and P. H. Haynes (1998), Internal interannual variability of the extratropical stratospheric circulation: The low-latitude flywheel, *Q. J. R. Meteorol. Soc.*, *124*, 2149–2173.

Semeniuk, K., and T. G. Shepherd (2001a), The middle-atmosphere Hadley circulation and equatorial inertial adjustment, *J. Atmos. Sci.*, *58*, 3077–3096.

Semeniuk, K., and T. G. Shepherd (2001b), Mechanisms for tropical upwelling in the stratosphere, *J. Atmos. Sci.*, *58*, 3097–3115.

Takahashi, M. (1996), Simulation of the stratospheric quasi-biennial oscillation using a general circulation model, *Geophys. Res. Lett.*, *23*, 661–664.

Takahashi, M. (1999), Simulation of the quasi-biennial oscillation in a general circulation model, *Geophys. Res. Lett.*, *26*, 1307–1310.

Tsuda, T., T. Murayama, M. Yamamoto, S. Kato, and S. Fukao (1990), Seasonal variation of momentum flux in the mesosphere observed with the MU radar, *Geophys. Res. Lett.*, *17*, 725–728.

Tsuda, T., M. Nishida, C. Rocken, and R. H. Ware (2000), A global morphology of gravity wave activity in the stratosphere revealed by the GPS occultation data (GPS/MET), *J. Geophys. Res.*, *105*, 7257–7273.

Tung, K. K., and J. S. Kinnersley (2001), Mechanisms by which extratropical wave forcing in the winter stratosphere induces upwelling in the summer hemisphere, *J. Geophys. Res.*, *106*, 22,781–22,791.

Watanabe, S., K. Sato, and M. Takahashi (2006), A general circulation model study of orographic gravity waves over Antarctica excited by katabatic winds, *J. Geophys. Res.*, *111*, D18104, doi:10.1029/2005JD006851.

Watanabe, S., Y. Kawatani, Y. Tomikawa, K. Miyazaki, M. Takahashi, and K. Sato (2008), General aspects of a T213L256 middle atmosphere general circulation model, *J. Geophys. Res.*, *113*, D12110, doi:10.1029/2008JD010026.

Wehrbein, W. M., and C. B. Leovy (1982), An accurate radiative heating and cooling algorithm for use in a dynamical model of the middle atmosphere, *J. Atmos. Sci.*, *39*, 1532–1544.

Wilson, R., M. L. Chanin, and A. Hauchecorne (1991), Gravity waves in the middle atmosphere observed by Rayleigh lidar. part 2: Climatology, *J. Geophys. Res.*, *96*, 5169–5183.

Wu, D. L., and J. W. Waters (1996), Satellite observations of atmospheric variances: A possible indication of gravity waves, *Geophys. Res. Lett.*, *23*, 3631–3634.

Yoshiki, M., and K. Sato (2000), A statistical study of gravity waves in the polar regions based on operational radiosonde data, *J. Geophys. Res.*, *105*, 17,995–18,011.

Yoshiki, M., N. Kizu, and K. Sato (2004), Energy enhancements of gravity waves in the Antarctic lower stratosphere associated with variations in the polar vortex and tropospheric disturbances, *J. Geophys. Res.*, *109*, D23104, doi:10.1029/2004JD004870.

Y. Kawatani, K. Miyazaki, and S. Watanabe, Frontier Research System for Global Change JAMSTEC, 3173-25 Showamachi, Kanazawa-ku, Yokohama, Kanagawa 236-0001, Japan.

K. Sato, Department of Earth and Planetary Science, Graduate School of Science, University of Tokyo, 7-3-1 Hongo, Bunkyo-ku, Tokyo 133-0033, Japan.

M. Takahashi, Center for Climate System Research, University of Tokyo, 5-1-5 Kashiwanoha, Chiba 277-8568, Japan.

Y. Tomikawa, National Institute of Polar Research, 1-9-10 Kaga, Itabashi, Tokyo 173-8515, Japan. (tomikawa@nipr.ac.jp)